Reinforced concrete walls detailed with shape memory alloys: recent experimental and numerical investigations

Ryan Hoult - Institute of Mechanics, Materials and Civil Engineering, UCLouvain, Louvain-la-Neuve, Belgium. ryan.hoult@uclouvain.be

João Pacheco de Almeida –Institute of Mechanics, Materials and Civil Engineering, UCLouvain, Louvain-la-Neuve, Belgium. joao.almeida@uclouvain.be

Matthieu B. Lezaack - Institute of Mechanics, Materials and Civil Engineering, UCLouvain, Louvain-la-Neuve, Belgium. matthieu.lezaack@uclouvain.be

Aude Simar - Institute of Mechanics, Materials and Civil Engineering, UCLouvain, Louvain-la-Neuve, Belgium. aude.simar@uclouvain.be

Abstract: The substitution of reinforcing steel with shape memory alloys has been offered as a solution for reducing residual displacements in reinforced concrete (RC) walls. This paper presents some recent experimental and numerical research efforts conducted by the authors and colleagues in the iMMC at UCLouvain focusing on the seismic performance of RC walls detailed with shape memory alloys. A summary of an experimental campaign is provided, which involved testing two large-scale planar RC walls. Some results from numerical simulations using state-of-the-art finite element modelling are also presented. Current and future research will focus, among others, on developing a more robust connection between the shape memory alloy and conventional steel rebars for implementation in concrete structures.

Keywords: SMA, residual-based, reinforcement, operational, serviceability

1. Introduction

In modern earthquake engineering, reinforced concrete (RC) walls are designed with the intention of providing sufficient strength and ductility (i.e., possibly large but controlled deformations) with the aim of avoiding collapse in case of a rare earthquake (Sritharan *et al.*, 2014). To provide the required strength, modern walls are designed with additional ("lumped") reinforcing steel at the boundary ends of the wall. The steel bars in these "boundary regions" are expected to perform inelastically to provide the required deformation capacity and energy dissipation. However, the plastic performance of the steel reinforcement in these boundary regions results in permanent damage and is typically the source of the residual displacements in RC buildings (i.e., the permanent relative deformation of a structure with respect to its foundation). For example, 25% of buildings in Christchurch, New Zealand were no longer vertical after the M_w 6.3 earthquake in 2011 (Muir-Wood, 2015), where 60% of RC buildings over three storeys were demolished because of extreme building tilts after being declared "uneconomic to repair" (Gonzalez *et al.*, 2021). While the primary performance level of no collapse for modern-designed RC structures can typically be achieved, the level of damage to structures and the economic losses are unexpectedly high (Goldsworthy, 2012). In the case of Christchurch, losses of more than $NZD 40 billion (i.e., 20% of the country's GDP) were accumulated from the event (Marquis *et al.*, 2017). The antiquated design philosophy of collapse prevention (or life safe), while deemed satisfactory to most engineers, no longer satisfies building owners and the public at large, whom are overwhelmed by the extent of damage, cordoning off of the city, and disruption of services (Goldsworthy, 2012). Thus, in addition to collapse prevention as a performance objective, sufficient attention needs to be paid to the post-earthquake reparability and serviceability of structures. While the former is primarily controlled by the peak inelastic displacement, the latter typically uses the residual displacement as an important criterion.

Shape Memory Alloys (SMAs) have been attracting some interest from researchers and structural engineers because of their ability to (i) recover displacements upon removal of stress, (ii) dissipate energy through hysteretic damping, and (iii) provide strength and displacement capacities comparable to conventional steel reinforcement (Abdulridha & Palermo, 2017). It is for these reasons that SMA bars have the potential to be used as reinforcement in wall boundary ends, aiming to reduce residual displacements and ultimately decrease societal and economic impacts after seismic events. The authors are aware of three separate experimental research investigations that tested RC walls detailed with SMA bars (Abdulridha & Palermo, 2017; Cortés-Puentes *et al.*, 2018; Kian & Cruz-Noguez, 2018). All three of these wall tests experienced some experimental or laboratory limitations that essentially restricted the seismic performance of these specimens, including: (i) no axial load was applied to all three wall specimens, which has been shown to greatly reduce the residual displacements (Dazio, 2004; Hoult & Almeida, 2022a; Maciel *et al.*, 2016) and (ii) small shear spans (i.e., ratio of wall height to length) were used for all three specimens, representing low-rise buildings only. Regarding the latter of these issues, the construction of considerably taller and more expensive units is not always possible (Holden *et al.*, 2003).

An experimental and numerical program was recently undertaken at Université catholique de Louvain (UCLouvain) in the Institute of Mechanics, Materials and Civil Engineering (iMMC) to investigate the seismic performance of RC walls detailed with SMA rebars. The experimental program included the testing of two large-scale (2:3) RC walls subjected to quasi-static cyclic loading protocols. In one specimen, ribbed steel rebars were replaced by nickel titanium (NiTi) SMA bars over a limited height above the base and inside the wall boundary element regions. The employed test setup allowed imposing an axial load as well as a large shear span, forcing the walls to behave in flexure as representative of medium to high-rise buildings. In the numerical program, an extensive number of walls were simulated using state-of-the-art finite element modelling. The purpose of this conference paper is to summarise some of the findings from these programs recently undertaken. Full details of these research investigations can be found in Almeida *et al.* (2020) and Hoult & Almeida (2022a,b). Finally, an overview of ongoing and future research being performed by the authors is also presented.

2. Summary of large-scale experimental tests

Two wall units at 2:3 scale with identical geometry were tested: A RC wall detailed completely with conventional steel (herein denoted specimen RC) was designed in accordance to the Eurocode 8 (CEN, 2004); an identical RC wall was also tested but detailed with four SMA rebars at the base of each boundary element (herein denoted as specimen RC+SMA). Each wall unit was 2000 mm tall, 200 mm thick, and 1200 mm long, and included a top loading beam (450 × 400 × 2400 mm^3) and a foundation block (600 × 400 × 2800 mm^3). Figure 1a illustrates some of the geometry and the reinforcement layout of the two test specimens. For the RC+SMA specimen, with detailing sketched on the right-half cross-sectional layout in Figure 1a, SMA rebars made of nickel titanium (NiTi) alloy were used with a diameter d_{bl} = 12.7 mm, which replaced the bottom 270 mm of longitudinal steel reinforcement in the wall. Mechanical couplers were used to connect the SMA and conventional steel rebars. More information regarding the specifics of the material and mechanical properties of the concrete, steel, and SMAs can be found in Almeida *et al.* (2020).

The test setup was assembled at the technological platform *Laboratoire Essais Mécaniques, Structures et Génie Civil* (LEMSC) of the iMMC at UCLouvain. The setup is shown in Figure 1b and consisted of two independent steel frames fixed to the laboratory strong floor, one supporting the vertical actuators and the other serving as a reaction frame for the horizontal actuator force. The vertical actuators apply an axial load of 350 kN to the specimens, corresponding to an axial load ratio (*ALR*) of 7.3%, as well as applying a varied bending moment that maintains a shear span ($M/VL_w = H_e/L_w$) of 3.6. The out-of-plane displacement at the height of the RC beam was prevented by using sliding supports that were attached to lateral bracing frames (represented in blue in Figure 1b). The horizontal actuator applied the reverse cyclic displacement history to the top RC beam of the specimens, which followed the quasi-static loading shown in Figure 2a and Figure 2b for RC and RC+SMA respectively. The loading protocol was displacement controlled, with each load stage an increment of drift until failure was determined.

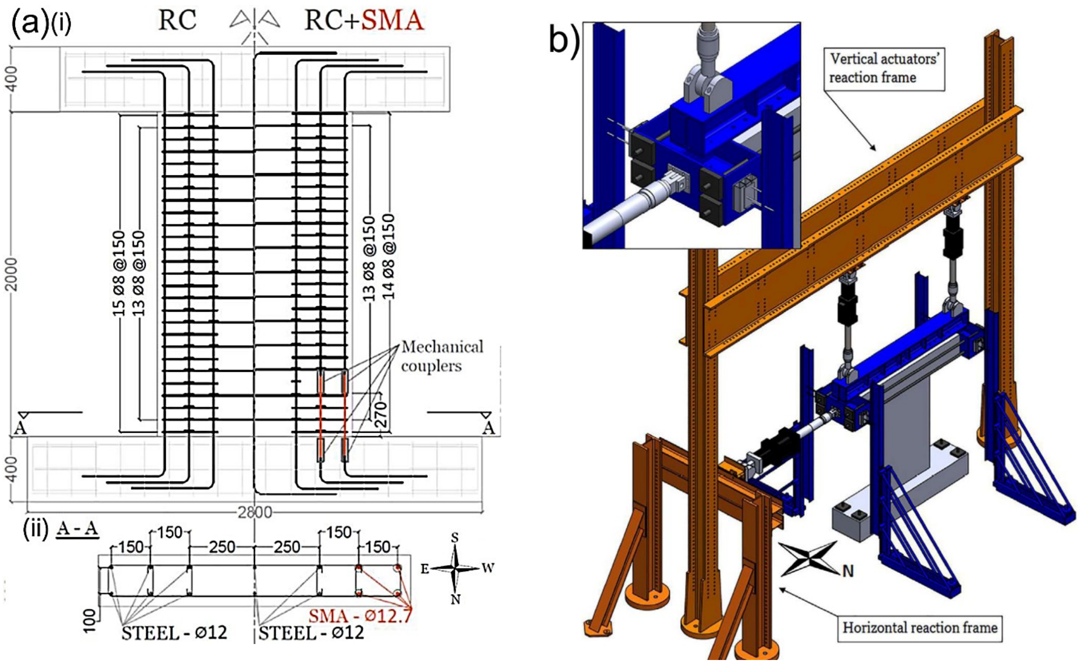

Figure 1 − (a) Geometry and reinforcement layout of test units RC and RC+SMA specimens, including close-up of the cross-section (b) 3D sketch of the setup assembled at the technological platform LEMSC for the test of the two walls

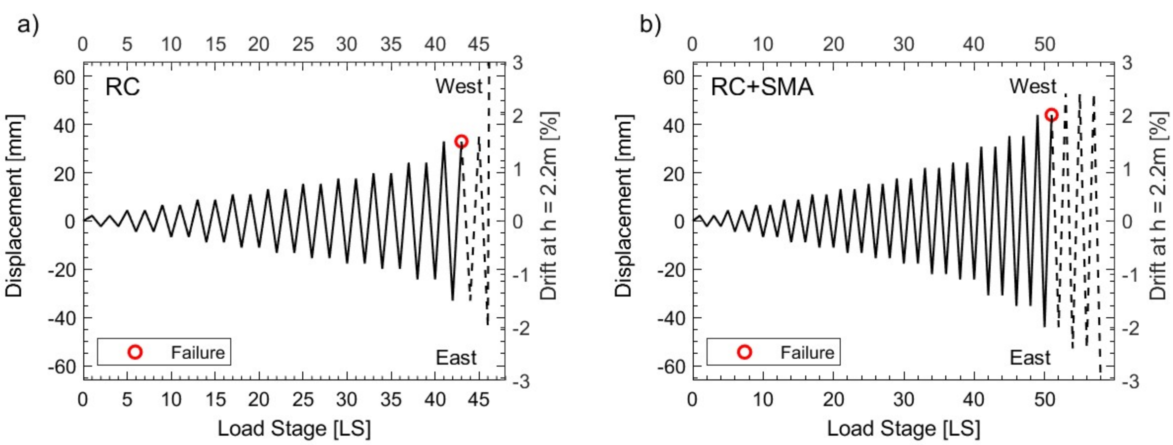

Figure 2 − (a) Loading protocol applied to specimen (a) RC and (b) RC+SMA

2.1. Response of specimen RC

A stable hysteretic response up to the specimen peak force was observed for the specimen detailed with conventional steel. An "explosive" noise could be heard while loading from -0.9% to 0.9% drift (i.e., from LS34 to LS35, Figure 2a), which corresponded to the formation of a large foundation cone and likely rebar fracture. The latter was accompanied by a sudden increase of the base crack width (at the tip of the cone), shown in Figure 3a, and corresponded to a reduction of widths of the cracks above this primary base crack. During loading towards LS41, at a drift of 1.37%, the sound of two additional rebar ruptures were perceived, corresponding to a drop in strength and onset of failure of this specimen. The test continued until the wall lost up to 70% of its maximum strength, along which five clear rebar rupture sounds were heard. Concrete crushing did not contribute to the drop in lateral strength and failure was entirely due to rebar rupture in the foundation. One of the reasons for the premature failure and much-reduced ductility capacity of this wall specimen included the relatively thin unit foundation block, which allowed the main base crack to dive into the foundation.

2.2. Response of specimen RC+SMA

An expected flag-shaped force-displacement response for specimen RC+SMA was observed. While progressing to a drift of 2.03% (i.e., LS49), steel rebar fracture could be heard, visibly causing a drop in the strength of the wall. It is likely that this steel rebar rupture was mixed with slipping of the SMA rebar in the coupler. Failure was attained during the second cycle at the same drift level (δ=2.03%, LS51), where another rebar rupture (i.e., rebar fracture) was distinctly heard and corresponded to a drop in strength. The response of this wall specimen indicated the activation of the superelastic SMA rebar behaviour while the stress in the steel rebars above the coupler remained below the yield stress. Unlike its RC counterpart, it was likely that concrete crushing, which developed in this specimen from drift levels of around 0.77% until drift at failure, contributed to the degradation of the strength observed (Figure 3b).

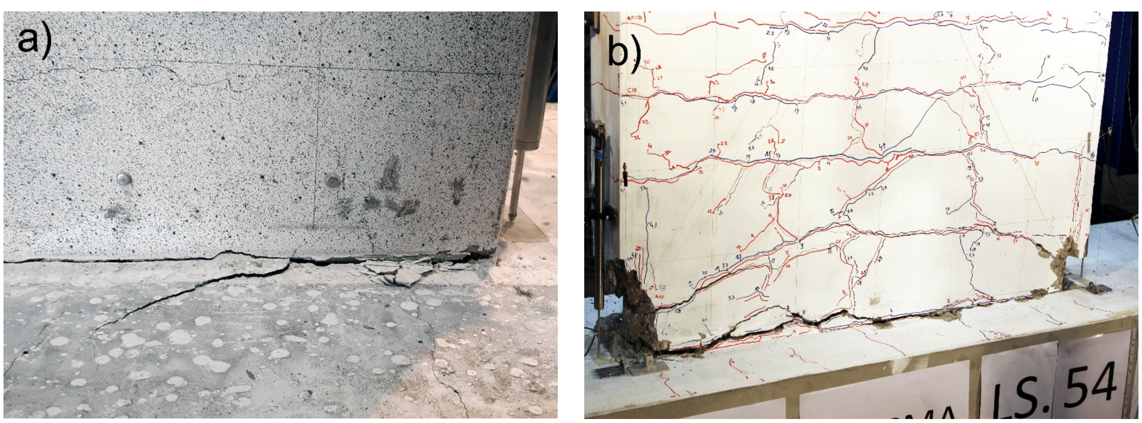

Figure 3 − (a) the base of specimen RC with formation of foundation cone and primary crack (LS35, δ=0.9%) and (b) damage state of specimen RC+SMA, including concrete crushing observed at the wall toe (LS54, δ=-2.4%)

The experimental force-displacement responses for both RC and RC+SMA specimens are shown in Figure 4a. Furthermore, the recorded residual displacements for both specimens are plotted in Figure 4b as a function of the in-plane drift. If the residual displacements are used as the engineering parameter to determine a wall's performance, then it is clear that the RC+SMA specimen performed much better than the RC specimen. Exponential lines-of-best-fit are also shown in Figure 4b to fit well to the results for both RC and RC+SMA

(r^2 correlations of 0.94 and 0.89, respectively). Superimposed in Figure 4b is a permissible residual drift limit of 0.005 rad (i.e., 0.5%), which is based on building functionality, construction tolerance levels, and structural safety (McCormick *et al.*, 2008). It can be observed that the permissible residual drift limit of 0.5% (=11mm for the current specimens) is reached at in-plane drifts of approximately 1% and 2% for the RC specimen and RC+SMA specimen respectively.

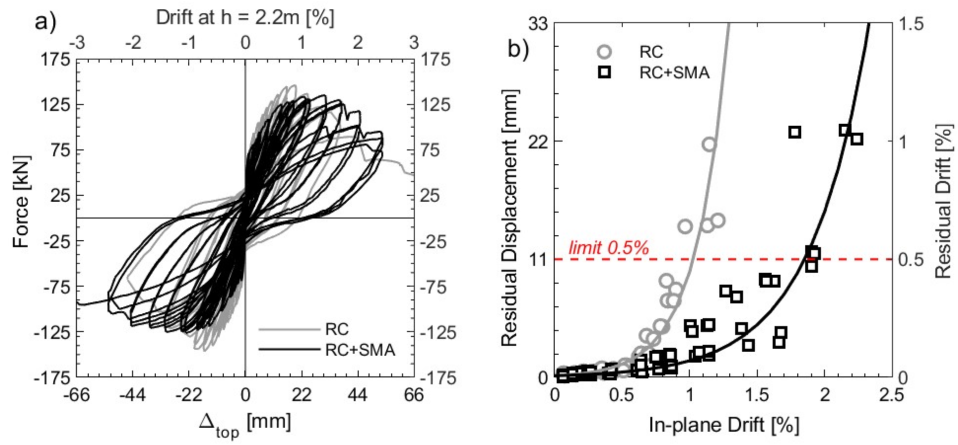

Figure 4 – Experimental results for both test specimens RC and RC+SMA (a) force-displacement hysteretic response and (b) residual displacement as a function of the in-plane drift

Digital image correlation (DIC) techniques were also used to determine the longitudinal strain distributed across the face of the walls using a base length of 100 mm. Micrometres were also used to determine a more accurate value of the tension strain at the base, which included the contribution of strain penetration into the foundation. Some of the resulting longitudinal strains are presented in Figure 5 in the form of heat maps. For specimen RC (Figure 5a), the longitudinal strains could only be calculated up to a wall height of 1200mm. At the drift level (δ) of 1.3%, there are some, albeit limited, distributed inelastic strains up the height of the wall prior to a concentration of strain at the base crack, which ultimately resulted in failure of this specimen governed by rebar rupture. The strain heat map for specimen RC at this drift level appears to be typical of a flexurally-governed wall, depicted by the pattern of predominantly horizontal stripes of higher longitudinal strains at different heights, corresponding to horizontal cracks (Figure 5a), with large tension or compression strains being reached in the respective extreme fibre regions. In contrast, specimen RC+SMA (Figure 5b) shows large inelastic strains accumulating throughout a greater length across the section of the wall and into the web. Note that the SMA rebar length at the base (to the mechanical coupler) is 270 mm. This type of strain distribution could explain the steel rebar ruptures heard during testing (Almeida *et al.*, 2020). Steel rebar rupture in, or close to, the web prior to the SMA bars in the boundary ends have also been reported in other testing on walls with similar detailing (Abdulridha & Palermo, 2017; Kian & Cruz-Noguez, 2018). There are several reasons that could explain this behaviour, which include the light amount of steel used to reinforce the web region of the wall, as well as the large differences in stiffness between the SMA rebars used in the extremities of the wall and the conventional steel used in the web (e.g., the elastic Young's modulus of the SMA and the steel is 31 GPa and 205 GPa, respectively).

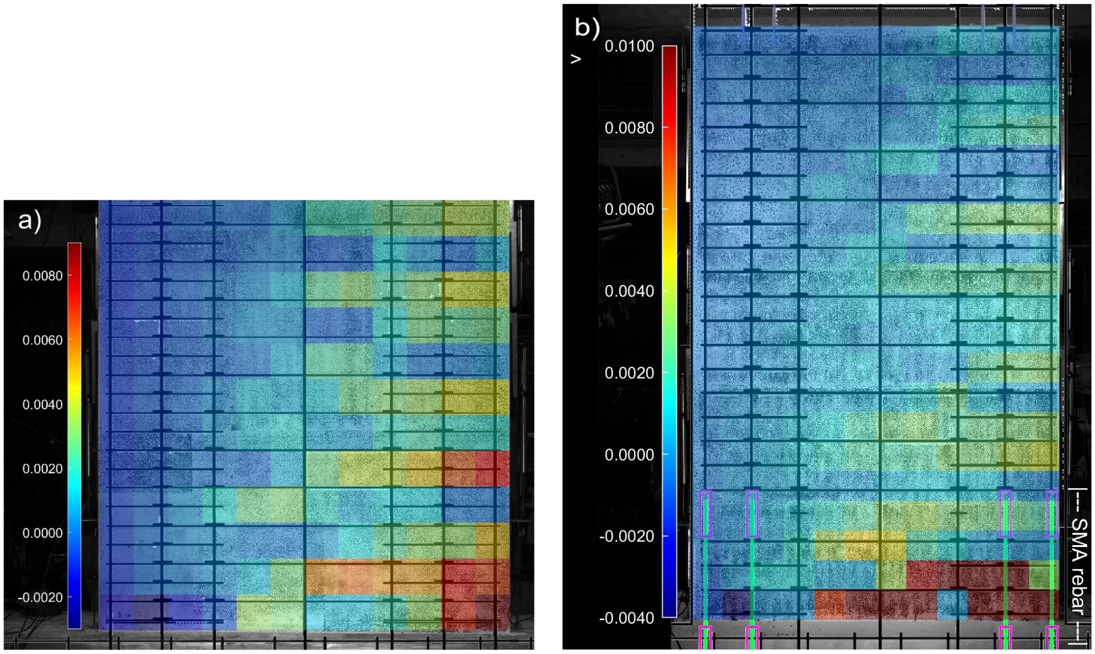

Figure 5 Heat map of longitudinal strains (a) RC, δ=1.3% and (b) RC+SMA, δ=1.4%

Using the automated-crack detection and crack measurement (ACDM) procedure (Gehri *et al.*, 2020, 2022), crack patterns and crack widths were determined for specimens RC and RC+SMA. The large base crack that formed between the foundation and the wall for both specimens has not been included in these analyses. As such, only the principal strains from the DIC data are used here. Figure 6 illustrates cracking distributions using the ACDM procedure for specimen RC and RC+SMA at similar drift levels. A reminder that only the lower 1200 mm of this wall specimen was captured using DIC techniques, and hence the top 800mm of the illustrated wall in Figure 6a,b has been shaded. Near-horizontal cracking occurs for the RC specimen (Figure 6a,b), which was initially noted in Almeida *et al.* (2020), confirming the predominantly flexural behaviour of the structure, as was expected from the large applied shear span ratio (of 3.6). At large enough drifts levels, the RC wall specimen appears to form a wide crack in the web of the wall (Figure 6b), which has been detailed with a relatively low amount of longitudinal steel. This large web crack, corresponding to high tensile strains in the web, can help to explain some of the rebar rupture sounds heard during testing. For specimen RC+SMA (Figure 6c,d), a large crack appears to form and extend upward from the base in the extreme tension fibre region and across into the web of specimen RC+SMA. In comparison to the crack widths determined for specimen RC at similar levels of drift, specimen RC+SMA is estimated to have smaller flexural crack widths in the extreme tension fibre region of the wall and up the wall height, consistent with the observed concentration of strain and plasticity at the base.

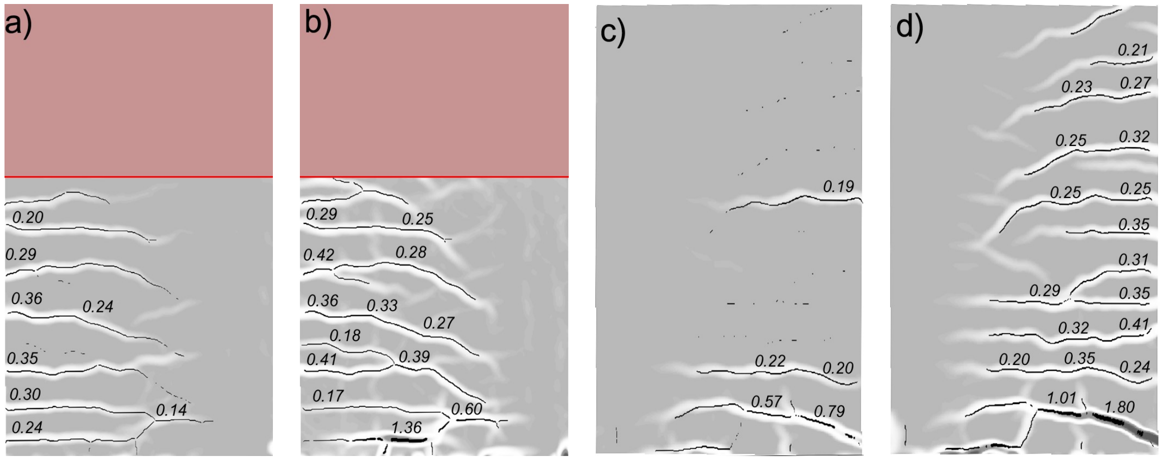

Figure 6 – Cracking distributions (a) RC, 0.4% (b) RC, 1.5%, (c) RC+SMA, 0.4%, (d) RC+SMA, 1.4% (note that the large base crack between foundation and the wall, for both specimens, is not depicted). The numbers superimposed in each of the figures are indicating the crack width below (in mm).

3. Numerical simulations

VecTor2 (Wong *et al.*, 2013), a state-of-the-art nonlinear finite element (FE) modelling program for plane RC sections that is based on the disturbed stress field model (DSFM) (Vecchio, 2000), is herein employed to simulate the wall unit RC+SMA tested at UCLouvain. Plane stress rectangular elements are used to model the concrete, which are four-noded elements with uniform thickness (Wong *et al.*, 2013). An element size corresponding to $0.33t_w$ is adopted for the walls based on the mesh sensitivity analysis undertaken in Hoult & Almeida (2022a), where t_w is the wall thickness. A maximum aspect ratio of 1.5 (Wong *et al.*, 2013) is used for the elements of the wall. The longitudinal SMA reinforcement in the boundary ends of the wall is modelled using truss-link elements, which allowed the simulation of the bond behaviour between the smooth rebars and the concrete. The Eligehausen (1983) bond stress-slip model was used to characterise the stress-slip behaviour of the smooth SMA rebars, which has been successfully used for this purpose in some previous numerical research (Abdulridha & Palermo, 2017; Soares *et al.*, 2021). The longitudinal steel reinforcement was modelled using truss elements, which assumes a perfect bond. The transverse reinforcement and confinement are modelled using smeared reinforcement throughout the concrete plane stress rectangular elements. Figure 7a illustrates the VecTor2 model of the RC+SMA wall specimen from Almeida *et al.* (2020). The material models are described in the study by Hoult *et al.* (2018), which are not repeated here for the sake of brevity. The full details and justifications for the chosen material models are provided in Hoult & Almeida (2022a). It is worth noting that, while the test specimen height was approximately 2200 mm (Figure 1), the VecTor2 model is extrapolated to a height that is equivalent to the shear span (Figure 7a), which was made possible experimentally with vertical actuators applying an overturning moment as mentioned above.

The numerical force-displacement response from VecTor2 for the RC-SMA specimen is illustrated in Figure 7b. Superimposed in this figure are the experimental results from Almeida *et al.* (2020). A very encouraging simulation of the force-displacement response of this wall is obtained numerically. As can be observed, the onset of failure, caused by rupturing of the outermost layer of reinforcing steel bars, occurred during the cycle towards a drift of approximately 2.4%, corresponding to a reduction in the force capacity. The VecTor2 simulations also provide reasonable estimates of the residual displacements of the wall, as indicated in Figure 7c, which is important for future studies investigating residual-based design measures. These results emphasise that it is possible to emulate the seismic response of RC-SMA walls to a fitting degree using state-of-the-art FE modelling. More information on the modelling procedure presented here, including further validation of the FE models using other experimental test results, can be found in Hoult & Almeida (2022b).

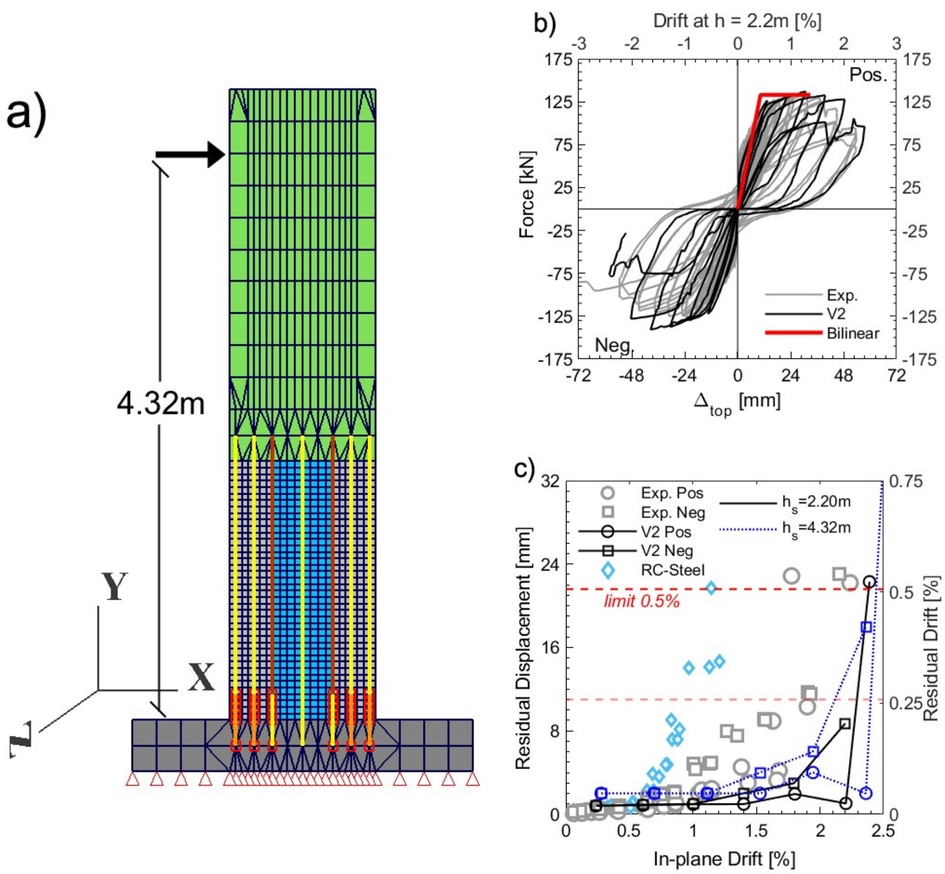

Figure 7 – (a) VecTor2 model of specimen RC+SMA (b) simulation of the force-displacement response (c) VecTor2 results of the estimated residual displacement

4. Current and future research

Mechanical couplers have been used in previous studies to connect the two different materials. In fact, all four tested RC-SMA wall specimens used mechanical couplers to connect the SMA rebars to conventional steel. The use of couplers has been also unavoidable for all beams, columns, and beam-column joints tested up to now (Raza *et al.*, 2022). There are, however, some challenges with the use of couplers in practice, including a reduction of RC member displacement capacity (Dahal & Tazarv, 2020); for example, up to 43% reduction has been reported when using mechanical couplers compared to unspliced members. Furthermore, the use of long, thick, and rigid couplers can restrict the rotation capacity of the RC member (Tazarv & Saiidi, 2016) and also impose some difficulties with regards to member detailing, including increased concrete covers and providing closely space confining reinforcement. Slippage inside the couplers has also been reported in several experimental tests (Raza *et al.*, 2022). It is for the above reasons that the current seismic codes prohibit the use of mechanical couplers within the plastic hinge regions of RC structures.

Thus, to avoid the use of couplers, the authors are currently developing a novel connection between SMA and steel rebars. A recent publication (Lezaack *et al.*, 2022), under review, demonstrates that a full-strength connection between NiTi SMA to conventional steel bars is possible through friction welding methods (Figure 8). While the performance of these connections was validated under quasi-static tensile monotonic loading, their response under dynamic, reverse-cyclic and fatigue loading is the subject of ongoing and future investigations, both under uniaxial tensile-compressive loading and as reinforcing rebars in RC structural members. The exploration of other materials within the SMA material family, namely Fe-based and Cu-based alloys, is also envisaged. The influence of the distinct axial stiffness between SMA and steel rebars on the evolution of the strain profiles along the length of RC walls – and its implications on structural performance and modelling – is also under investigation.

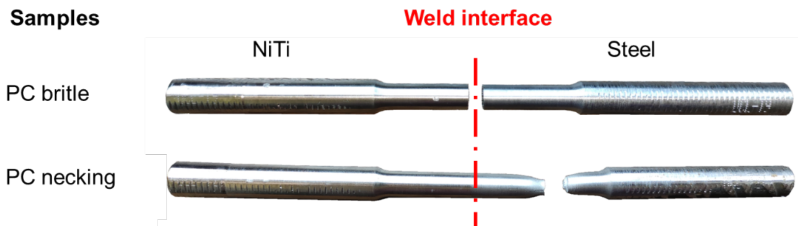

Figure 8 – Tensile samples of the NiTi SMA and steel bars joined through friction welding (Lezaack *et al*., 2022). Position control (PC) machine. Necking samples show fracture strength similar to the steel rebars.

5. Conclusions

A mix of experimental and numerical research investigations performed recently and ongoing at UCLouvain, focusing on the seismic performance of RC walls detailed with shape memory alloy rebars, was presented. The primary focus of detailing concrete structures with SMA materials is ultimately to reduce the residual displacements after these structures are subjected to ground motions from large earthquake events. Firstly, a summary of two wall specimens tested at the LEMSC laboratory of the iMMC is discussed. These wall tests showed the intended effective reduction of residual displacements for high shear span ratios characteristic of medium-to-high rise buildings and helped validating numerical models using state-of-the-art finite element modelling for simulating the performance of RC-SMA walls. However, there are some impediments to get around before SMA materials are readily adopted by construction practices internationally. One of these obstacles includes the continued use of mechanical couplers, which are not accepted by current building codes within plastic hinge regions. Continued research in this area is being conducted by the authors and colleagues at UCLouvain to develop a novel and robust connection that will make it easier to implement in future practices. It relies on a more fundamental connection at a material level which can help overcome the limitations and doubts regarding the currently employed mechanical bar splices. Other future work includes the characterization of the response, both at the connection and structural levels, for fatigue loading and dynamic low-cycle large-amplitude loading.

Acknowledgments

This work was supported by the Fonds de la Recherche Scientifique – FNRS under Grant nº F.4501.21.

References

Abdulridha, A., & Palermo, D. (2017). Behaviour and modelling of hybrid SMA-steel reinforced concrete slender shear wall. *Engineering Structures, 147*, 77-89. doi:10.1016/j.engstruct.2017.04.058

Almeida, J. P. d., Steinmetz, M., Rigot, F., & de Cock, S. (2020). Shape-memory NiTi alloy rebars in flexural-controlled large-scale reinforced concrete walls: Experimental investigation on self-centring and damage limitation. *Engineering Structures, 220*, 110865. doi:10.1016/j.engstruct.2020.110865

Cortés-Puentes, L., Zaidi, M., Palermo, D., & Dragomirescu, E. (2018). Cyclic loading testing of repaired SMA and steel reinforced concrete shear walls. *Engineering Structures, 168*, 128-141.
Dahal, P. K., & Tazarv, M. (2020). Mechanical bar splices for incorporation in plastic hinge regions of RC members. *Construction and Building Materials, 258*, 120308.
Dazio, A. (2004). *Residual displacements in capacity designed reinforced concrete structures.* Paper presented at the The 13th world conference on earthquake engineering, Vancouver, BC, Canada.
Eligehausen, R. (1983). Local bond stress-slip relationships of deformed bars under generalized excitations : experimental results and analytical model. In E. P. Popov & V. V. Bertero (Eds.). Berkeley, Calif. Earthquake Engineering Research Center, College of Engineering, University of California.
Gehri, N., Mata-Falcón, J., & Kaufmann, W. (2020). Automated crack detection and measurement based on digital image correlation. *Construction and Building Materials, 256*, 119383. doi:10.1016/j.conbuildmat.2020.119383
Gehri, N., Mata-Falcón, J., & Kaufmann, W. (2022). Refined extraction of crack characteristics in large-scale concrete experiments based on digital image correlation. *Engineering Structures, 251*, 113486. doi:10.1016/j.engstruct.2021.113486
Goldsworthy, H. M. (2012). Lessons on building design from the 22 February 2011 Christchurch earthquake. *Australian Journal of Structural Engineering, 13*(2), 159. doi:10.7158/S11-136.2012.13.2
Gonzalez, R., Stephens, M., Toma, C., Elwood, K., & Dowdell, D. (2021). Post-earthquake Demolition in Christchurch, New Zealand: A Case-Study Towards Incorporating Environmental Impacts in Demolition Decisions. In *Advances in Assessment and Modeling of Earthquake Loss* (pp. 47-64).
Holden, T., Restrepo, J., & Mander, J. B. (2003). Seismic performance of precast reinforced and prestressed concrete walls. *Journal of Structural Engineering, 129*(3), 286-296.
Hoult, R., Goldsworthy, H., & Lumantarna, E. (2018). Plastic Hinge Length for Lightly Reinforced Rectangular Concrete Walls. *Journal of Earthquake Engineering, 22*(8), 1447-1478. doi:10.1080/13632469.2017.1286619
Hoult, R. D., & de Almeida, J. P. (2022a). Residual displacements of reinforced concrete walls detailed with conventional steel and shape memory alloy rebars. *Engineering Structures, 256*, 114002. doi:10.1016/j.engstruct.2022.114002
Hoult, R., & Almeida, J. (2022b). RC walls detailed with shape memory alloys: new experimental findings. *Engineering Structures*.
Kian, M. J. T., & Cruz-Noguez, C. (2018). Reinforced Concrete Shear Walls Detailed with Innovative Materials: Seismic Performance. *Journal of Composites for Construction, 22*(6), 04018052. doi:10.1061/(ASCE)CC.1943-5614.0000893
Lezaack, M. B., Simar, A., Marchal, Y., Steinmetz, M., Faas, K., & Almeida, J. P. d. (2022). Dissimilar friction welding of NiTi shape memory alloy and steel reinforcing bars for seismic performance. *Submitted to Science and Technology of Welding and Joining*.
Maciel, M., Palermo, D., & Abdulridha, A. (2016). Seismic Response of SMA Reinforced Shear Walls. *Special Topics in Structural Dynamics, 6*, 185-192. doi:10.1007/978-3-319-29910-5_19
Marquis, F., Kim, J. J., Elwood, K. J., & Chang, S. E. (2017). Understanding post-earthquake decisions on multi-storey concrete buildings in Christchurch, New Zealand. *Bulletin of Earthquake Engineering, 15*(2), 731-758. doi:10.1007/s10518-015-9772-8
McCormick, J., Aburano, H., Ikenaga, M., & Nakashima, M. (2008). *Permissible residual deformation levels for building structures considering both safety and human elements.* Paper presented at the Proceedings of the 14th world conference on earthquake engineering, Beijing, China.
Muir-Wood, R. (2015). The Christchurch earthquakes of 2010 and 2011. The Geneva risk reports. Risk and insurance research. Extreme events and insurance: 2011 Annus horribilis. Courbage C, Stahel WR, Geneva.
Raza, S., Shafei, B., Saiidi, M. S., Motavalli, M., & Shahverdi, M. (2022). Shape memory alloy reinforcement for strengthening and self-centering of concrete structures—State of the art. *Construction and Building Materials, 324*, 126628.
Soares, M. M., Palermo, D., & Cortés-Puentes, W. L. (2021). Modelling of mid-rise concrete shear walls reinforced with superelastic shape memory alloys: Nonlinear analysis. *Engineering Structures*, *247*, 113049.
Sritharan, S., Beyer, K., Henry, R. S., Chai, Y. H., Kowalsky, M., & Bull, D. (2014). Understanding Poor Seismic Performance of Concrete Walls and Design Implications. *Earthquake Spectra, 30*(1), 307-334. doi:10.1193/021713EQS036M
Tazarv, M., & Saiidi, M. S. (2016). Seismic design of bridge columns incorporating mechanical bar splices in plastic hinge regions. *Engineering Structures, 124*, 507-520.
Wong, P., Vecchio, F., & Trommels, H. (2013). Vector2 and FormWorks User Manual. Department of Civil Engineering, University of Toronto.